Energy Separation between Quartet and Doublet Spin States of Radical−Triplet Encounter Pairs; Unusual Ferromagnetic Interaction in a 1,1-Diphenyl-2-picrylhydrazyl and Triplet Coronene Pair

Akio Kawai[†,‡,§] and Kazuhiko Shibuya*[,†]

Department of Chemistry, Graduate School of Science and Engineering, Tokyo Institute of Technology, 2-12-1 Ohokayama, Meguro-ku, Tokyo 152-8551, Japan, and PRESTO, Japan Science and Technology Corporation, Kawaguchi, Saitama 332-0012, Japan

Received: July 22, 2002; In Final Form: October 8, 2002

Time-resolved ESR (TR-ESR) measurements were performed for chemically induced dynamic electron polarization (CIDEP) created in various systems of the 1-diphenyl-2-picrylhydrazyl (DPPH) radical and triplet organic molecules. TR-ESR spectra of DPPH show a net emission CIDEP signal in most of the DPPH−triplet systems. The only exception was observed for a DPPH−coronene system in which the TR-ESR spectrum of DPPH presents a net absorption CIDEP signal. The origin of these net emission and absorption CIDEP signals is interpreted in terms of the radical−triplet pair mechanism (RTPM) for a triplet quenching process. To confirm that the CIDEP is created by RTPM, we simulated the time profiles of the TR-ESR signal with modified Bloch and kinetic equations. Stern−Volmer type analyses of the CIDEP intensities also support the assignment for the proposed CIDEP mechanism. According to the signal sign rule in RTPM, we examined the energy difference, *J*, of the quartet and doublet spin states of the radical−triplet encounter pair (RTP). *J* is defined by the equation $J = E(^2\text{RTP}) - E(^4\text{RTP})$ where $E(^2\text{RTP})$ and $E(^4\text{RTP})$ represent the energies of doublet and quartet RTP states, respectively. According to the CIDEP signal, most of the RTPs in DPPH−triplet molecule systems show a normal negative *J*-value, while a DPPH−triplet coronene pair shows an unusual positive *J*-value. The mechanism for this unusual antiferromagnetic coupling in the DPPH−triplet coronene pair is explained by introducing an intermolecular charge-transfer interaction.

Introduction

The encounter of paramagnetic species such as radicals and triplet molecules is accompanied by the intermolecular interaction to induce energy separation between resultant spin states with different spin multiplicity. For example, singlet−triplet and doublet (|D>)−quartet (|Q>) separations have been observed for radical pairs and radical−triplet (RT) pairs, respectively. The energy difference of separated states is usually described by a *J*-value, where *J* is defined by the equation, $J = E(^m\text{Pair}) - E(^n\text{Pair})$ with $m < n$, where $E(^m\text{Pair})$ and $E(^n\text{Pair})$ mean the energies of the pairs of paramagnetic species with spin multiplicities of *m* and *n*, respectively. The energy separations are essentially related to the magnetic properties of these complexes and it is interesting to understand the mechanisms determining the *J*-value. A large number of studies concerning the *J*-value have been reported on radical pairs[1−3] and RT pairs[4−10] utilizing a time-resolved ESR (TR-ESR) method. For the TR-ESR study of the *J*-value, there are direct and indirect methods, which are briefly explained below.

In the direct observation, the spectra of the spin-correlated pair of paramagnetic species themselves are measured and analyzed to obtain the information of the *J*-value. As for radical pairs, there are many studies taking the spectra of spin-correlated radical pairs such as an acetone ketyl pair,[1] a benzophenone ketyl pair in an SDS micelle,[2] and so on.[3] Simulations of the observed spectra gave us details of magnetic interactions within radical pairs in addition to the determination of *J*-values. Although the direct method is quite simple and convincing, there is a disadvantage in that this method requires long-lived stable pairs and well-resolved spectra with sharp lines overcoming the broadening due to tumbling and diffusion motion of the encounter pair. Hence, this method is valid for limited pairs. Unfortunately, no successful observations of the ESR spectra of RT encounter pairs (RTP) have been reported.

In the indirect observation, chemically induced dynamic electron polarization (CIDEP) of free paramagnetic species is measured after CIDEP is created by the magnetic interactions between the paramagnetic species at the encounter pair distance.[11] Even after the encounter pair diffuses apart, CIDEP created during the encounter period is conserved for a few microseconds which is long enough to be detected by a TR-ESR method. In studies by the indirect method, the sign of the *J*-value is judged by the phase of CIDEP on the basis of CIDEP mechanisms.

Our interest in this work lies in the *J*-value of RTPs which has recently attracted much attention in the studies of interactions of paramagnetic species. So far, *J*-values of RTP have been studied only by the observation of CIDEP. We describe how *J*-values are examined on the basis of CIDEP measurements. Figure 1 shows a schematic description for the relation between the sign of the *J*-value and the CIDEP phase in an RT system. Upon RT encounter, CIDEP of the radical in α-spin and β-spin enriched populations are created for negative and

* Corresponding author. Tel: +81-3-5734-2231. Fax: +81-3-5734-2655. E-mail: kshibuya@chem.titech.ac.jp.
† Tokyo Institute of Technology.
‡ PRESTO, Japan Science and Technology Corporation.
§ E-mail: akawai@chem.titech.ac.jp.

10.1021/jp021689s CCC: $22.00
Published on Web 11/28/2002

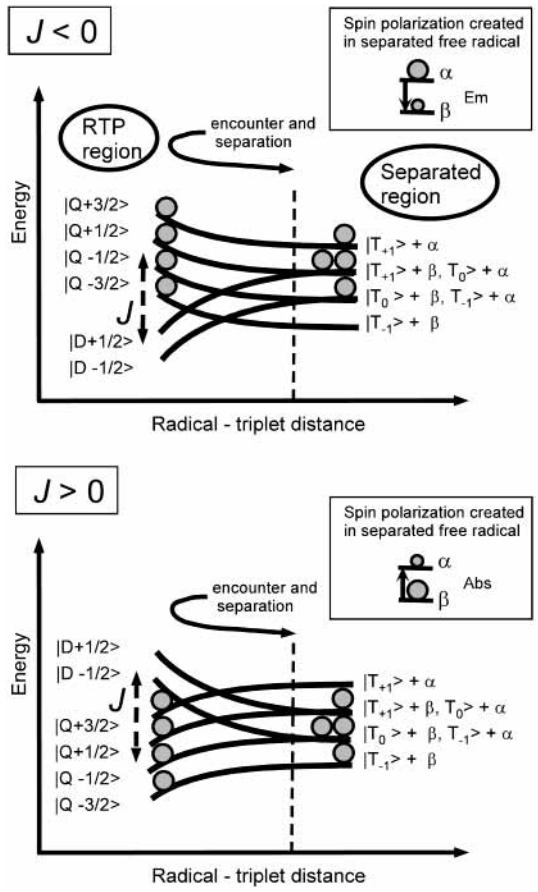

Figure 1. Schematic description of RTPM and the *J*-value for energy separation between the quartet ($|Q \pm 1/2, \pm 3/2\rangle$) and doublet ($|D \pm 1/2\rangle$) spin states of the RT encounter complex under an external magnetic field. The spin states of the triplet molecule and doublet radical separated from RTP are denoted as $|T_0, \pm 1\rangle$ and α (or β), respectively. The CIDEP phase of radical is in Em (α-spin-enriched population) for $J < 0$ or is in Abs (β-spin-enriched population) for $J > 0$, after the separation of the equally populated quartet spin-substates of the encounter complex.

positive *J*-values, respectively, according to the theory of the RT pair mechanism (RTPM).[4,6,12] The resultant CIDEP signal is in phase of emission (Em) or absorption (Abs) as illustrated in the insets of Figure 1. Therefore, the phase of CIDEP created by RTPM tells us the sign of the *J*-value. After a comprehensive set of TR-ESR studies to determine the signs of the *J*-value in RTP, it was found that the majority of the pairs show antiferromagnetic coupling giving a negative sign of the *J*-value. The radicals examined includes chemically stable radicals (nitroxide[5−7] and galvinoxyl[8,9]) and photochemical intermediate species (ketyl radical of aromatic ketones and naphthoxy radicals[6,10]). These results have been in line with the singlet−triplet splitting mechanism in the radical pairs in which most of the pairs indicate antiferromagnetic coupling.

We have recently discovered that some galvinoxyl−triplet molecule pairs show ferromagnetic interaction, namely, the |D> states of RTP lie above the |Q> states.[8] This is the first observation where the RTP show positive *J*-values. This abnormal observation was explained by introducing an intermolecular charge transfer (CT) interaction in addition to the exchange interaction between radical and triplet molecules. Spin-selective electronic coupling between the doublet RTP and CT states results in the energy shift of the |D> state. According to this energy shift, relative energy between the |Q> and |D> states of RTP changes and, in some systems, the |D> state locates above the |Q> state. We examined the sign of the *J*-value against the energy gap between zero-order CT (CT^0) and RTP (RTP^0) states,[8] where the electronic coupling between the doublet RTP^0 and CT^0 states was neglected. The unusual positive sign of the *J*-value was found to appear only in the system where the energy gaps are around $0 \sim -15$ kcal mol^{-1}. On the contrary to the study on RTPs with galvinoxyl, no positive *J*-values were found in tetramethylpiperydyl-oxy (TEMPO)−triplet molecule systems though we examined the *J*-value of the systems in a wide range of energy gap values. A discovery of positive *J*-values in the RTPs of galvinoxyl−triplet molecule systems encouraged us to continue our search for the *J*-value of RTPs. In the present study, we used the 1,1-diphenyl-2-picrylhydrazyl (DPPH) radical which is known as another chemically stable free radical, and measured the sign of the *J*-value in various DPPH−triplet molecule systems.

First of all, we analyzed the CIDEP mechanism of DPPH created in the DPPH−triplet molecule systems. In RT systems, there exist two distinct CIDEP mechanisms; one is RTPM as described above and the other is electron-spin polarization transfer (ESPT) from the spin-polarized triplet to the free radical during the spin exchange process at RT encounter.[9,13] If CIDEP is created by RTPM, we are able to determine the sign of the *J*-value from the CIDEP phase. If CIDEP is created by ESPT, the CIDEP phase does not indicate the sign of the *J*-value and it is not possible to determine the sign of the *J*-value. In this work, we performed a detailed analysis of CIDEP time evolution on the basis of the Bloch equation and Stern−Volmer analysis of CIDEP intensities in the DPPH−triplet molecule systems and conclude that all the CIDEP observed are dominantly created by RTPM. Therefore, we were able to apply the sign rule of RTPM for the CIDEP to determine the sign of the *J*-value. Finally, we gave a conclusion that most of the system shows a negative *J*-value as is similar to the case of TEMPO−triplet molecule systems while DPPH−triplet coronene system shows an unusual positive *J*-value. An energy gap plot for the *J*-value is performed for the results and an effect of CT state on the *J*-value in DPPH−triplet molecule systems is discussed.

Experimental Section

TR-ESR signals were detected by conventional X-band ESR spectrometers (Bruker, ELEXIS 580E or Varian E112) combined with a boxcar integrator (Stanford, SR-250) for spectra or a digital oscilloscope (SONY/Techtroniks, TDS340) for time profiles. The excitation UV lights were 355 nm by the third harmonics of a YAG laser (Continuum, Powerlight 8000) or 297 nm by the frequency doubling (Inrad, R-6G crystal) of a dye laser (Lambda Physik, Scanmate) pumped by the second harmonics of the YAG laser (532 nm 100mJ/pulse). The laser power was attenuated to be about 0.2 mJ/pulse at 297 nm and about 2−3 mJ/pulse at 355 nm. The signals were collected at the repetition rate of 10 Hz. The microwave power was usually 15−30 mW. A wide-band preamplifier (Bruker, ER047PH) was used for time profile measurements to determine triplet quenching rate constants. All the chemicals (Tokyo Kasei) were used as received. The concentration of DPPH was 0.25−0.7 mM (M = mol dm^{-3}). Sample solutions were degassed by bubbling Ar gas unless otherwise mentioned and were flowed through a quartz flat cell with 0.5 or 0.7 mm interior space. All the measurements were carried out at room temperature (293 K).

Results and Discussion

CIDEP Created in DPPH−Triplet Molecule Systems. First of all, we measured the absorption spectrum of DPPH as shown

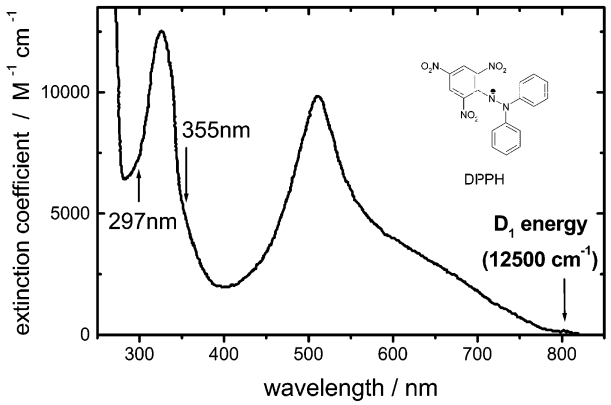

Figure 2. Absorption spectrum of DPPH in benzene at 293 K.

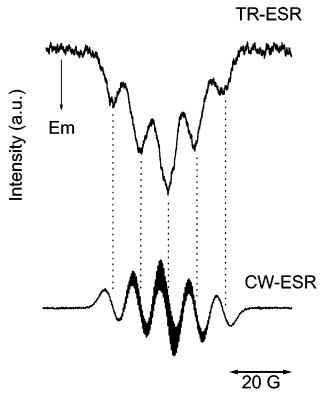

Figure 3. TR-ESR spectrum of DPPH observed with the 355 nm laser excitation of the DPPH(0.51 mM)/9-fluorenone(28 mM) system in benzene. The gate was opened for 1.5−2.0 μs after laser excitation. The CW-ESR spectrum of DPPH was obtained for the same sample solution without laser excitation.

in Figure 2. Compared to the absorption spectra of free radicals such as galvinoxyl and TEMPO previously used in our studies, the most remarkable character of this spectrum lies in the large extinction coefficients of DPPH in the visible and UV spectral region. The strong absorption of DPPH starts at 820 nm and displays two remarkable peaks at 510 and 325 nm. No additional absorption could be recognized in the longer wavelength region of 820−900 nm. We attributed a band starting at 820 nm to the D_1-D_0 transition and determined the D_1 energy to be 12200 cm^{-1}. For CIDEP measurements, it is desirable to photoexcite singlet molecules, which are triplet precursors, without excitation of the free radical. The excitation light wavelength was selected to be 355 or 297 nm, depending on triplet precursor molecules, to avoid the light absorption due to the intense band of DPPH around 325 nm. Despite the laser-excited DPPH, no CIDEP signals appeared in the absence of triplet precursor molecules. This means that the photochemistry of DPPH itself is not important in the present CIDEP measurements. Absorbance of DPPH at 297 nm is calculated to be about 0.35 at the concentration of 1 mM. In our experiments, the DPPH concentration was less than 0.7 mM to minimize the direct excitation of DPPH.

Figure 3 shows a TR-ESR spectrum obtained by the 355 nm laser excitation of 9-fluorenone in the benzene solution of DPPH and 9-fluorenone. The spectrum is characterized by a broad quintet hyperfine structure, which is exactly the same as that of the CW-ESR spectrum of DPPH. Therefore, we assigned this TR-ESR spectrum to be due to the CIDEP of the DPPH radical. We measured a series of TR-ESR spectra of DPPH in various DPPH-excited molecule systems, some of which are

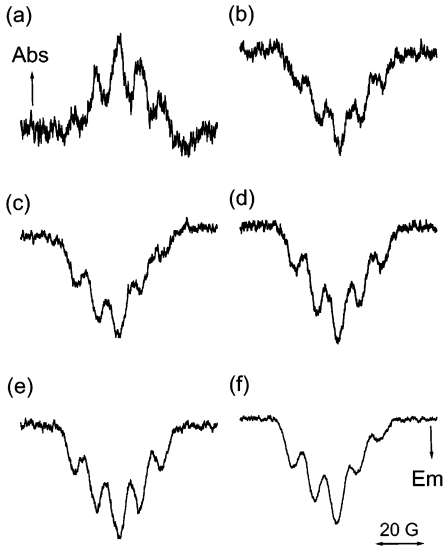

Figure 4. TR-ESR spectra of DPPH observed with the 355 nm laser excitation of various samples. The samples are (a) DPPH(0.71 mM)/coronene(5.5 mM) in anisole, (b) DPPH(0.39 mM)/benzil(48 mM) in benzene, (c) DPPH(0.61 mM)/fluoranthene(18 mM) in toluene, (d) DPPH(0.64 mM)/benzophenone(137 mM) in benzene, (e) DPPH(0.33 mM)/2-nitronaphthalene(17 mM) in benzene, and (f) DPPH (0.40 mM)/tetraphenylporphine(3.4 mM) in toluene.

TABLE 1: Summary of CIDEP Phases and Estimated Encounter Probability of DPPH and the S_1 Molecules

molecules	CIDEP phase	τ_f/ns[a]	DPPH−S_1 encounter probability[b]	wavelength/nm (solvent)
pyrene	Em	450	0.7	355 (benzene)
coronene	Abs	240	0.3	355 (anisole)
naphthalene	Em	96	0.2	297 (cyclohexane)
phenanthrene	Em	58	0.2	297 (toluene)
fluoranthene	Em	53	0.2	355 (toluene)
tetraphenylporphine	Em	13.6	0.06	355 (toluene)
9-fluorenone	Em	2.8	0.01	355 (benzene)
benzil	Em	2.0	0.01	355 (benzene)
benzophenone	Em	0.03	0.00	355 (benzene)
quinoxaline	Em	0.023	0.00	297 (toluene)
phenazine	Em	0.014	0.00	355 (benzene)
2-nitronaphthalene	Em	0.010	0.00	355 (benzene)

[a] The τ_f values are obtained from ref 14; the τ_f value of coronene was measured by the S_1-S_n absorption decay in the present study.[b] The encounter probability was estimated by k_{diff} [DPPH]/($\tau_f^{-1} + k_{diff}$ [DPPH]) where k_{diff} means the diffusion rate constants of 1.0×10^{10}, 1.1×10^{10}, 0.49×10^{10}, and 0.67×10^{10} M^{-1} s^{-1} for benzene, toluene, anisole, and cyclohexane, respectively, using the viscosities in ref 14.

shown in Figure 4. Most of the systems show net signals in the Em phase, with a very minor modification in the hyperfine intensity pattern. Only the coronene system shows an Abs signal phase. The observed TR-ESR signal phases are listed in Table 1.

To estimate the contribution of the S_1 state to the TR-ESR signal, we calculated the probability for the S_1 state molecule to encounter DPPH at a diffusion-controlled rate. The resultant encounter probabilities are summarized in Table 1. As seen from Table 1, the molecules listed in the top 5 rows (pyrene−fluoranthene) have encounter probabilities above 20%. The molecules tabulated in the bottom 7 rows (tetraphenylporphine−2-nitronaphthalene) show encounter probabilities of less than 10% and we neglected the effect of DPPH−S_1 molecule interaction. The triplet lifetimes of all the molecules listed in Table 1 are more than 10 μs[15] and the encounter probability of triplet molecules with DPPH is close to 100%. Therefore, we

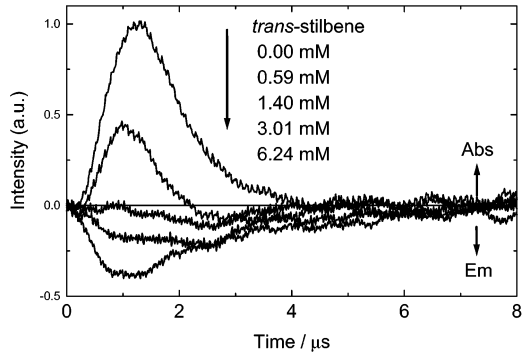

Figure 5. Time profiles of the TR-ESR signal of DPPH observed with the 355 nm excitation of the DPPH(0.29 mM)/coronene(3.3 mM) systems in anisole with various concentrations of *trans*-stilbene. The signal was measured at the central peak of the TR-ESR spectrum of DPPH shown in Figure 3.

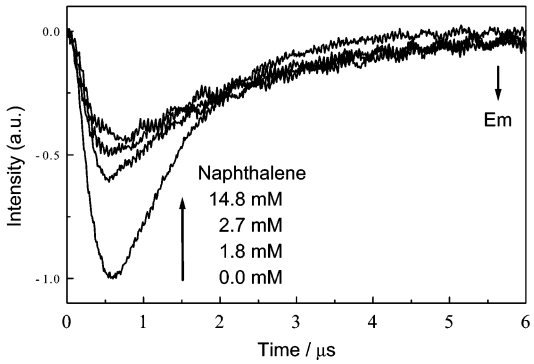

Figure 6. Time profiles of the TR-ESR signal of DPPH observed with the 355 nm laser excitation of the DPPH(0.58 mM)/benzophenone(74 mM) system in benzene with various concentrations of naphthalene.

concluded that the DPPH−triplet molecule encounter is dominant in CIDEP creation for the molecules tabulated in the bottom 7 rows of Table 1. For pyrene, coronene, naphthalene, phenanthrene, and fluoranthene, it is not straightforward to tell which encounter process of DPPH with the S_1 or the T_1 is important in CIDEP creation. Therefore, we performed the following CIDEP measurements in the presence of a triplet quencher or triplet photosensitizer.

For the pyrene, coronene, and fluoranthene systems, the 355 nm excitation with *trans*-stilbene as a triplet quencher was employed, since *trans*-stilbene does not absorb 355 nm light and the quenching rates of these triplet molecules by *trans*-stilbene are very fast due to the exothermic T_1-T_1 energy transfer processes.[14] Figure 5 shows the time profiles of the TR-ESR signal measured in a DPPH−coronene system with various concentrations of *trans*-stilbene. The Abs signal of DPPH simply rises and decays in the absence of *trans*-stilbene. With increasing *trans*-stilbene concentration, the Abs signal of DPPH decreases in intensity and finally turns over to a weak Em signal. The encounter pair of DPPH and triplet *trans*-stilbene may create this Em signal. The fluorescence of coronene was not quenched by *trans*-stilbene even at the high concentration of 0.1 M. On the other hand, Figure 5 clearly indicates that the Abs signal created in the DPPH−coronene system is quenched out by *trans*-stilbene even at the low concentration of 1.4 mM. These results lead us to conclude that the Abs signal created in the DPPH−coronene system is not due to the DPPH−S_1 coronene pair but is due to the DPPH−triplet coronene pair. As recognized at the *trans*-stilbene concentration of 0.59 mM in Figure 5, the Abs signal of DPPH displays a simple rise and decay followed by the weak Em signal. The Abs signal is created by the DPPH−triplet coronene pair after the photoexcitation, while the signal phase changes to Em created by the DPPH−triplet *trans*-stilbene pair after the T_1-T_1 energy transfer from coronene to *trans*-stilbene. The quenching of TR-ESR signal by *trans*-stilbene was also observed in the fluoranthene and pyrene systems and we conclude that CIDEP of DPPH in these molecular systems are created by the DPPH−triplet molecule pairs.

For the naphthalene and phenanthrene systems, *trans*-stilbene is not available as a triplet quencher because the S_1 energies of these molecules are close to that of *trans*-stilbene and selective excitation of naphthalene or phenanthrene is impossible. We performed triplet sensitization experiments in which triplet benzophenone is selectively prepared by the 355 nm excitation followed by the T_1-T_1 energy transfer from benzophenone to naphthalene or phenanthrene. Figure 6 shows decays of the TR-ESR signal of DPPH in a benzophenone/naphthalene mixture system with DPPH. In the absence of naphthalene, a strong Em signal created by a DPPH−triplet benzophenone pair was observed. In the presence of naphthalene, rapid T_1-T_1 energy transfer occurs[16] with the rate constant of 4.7×10^9 M^{-1} s^{-1}. Since the concentration of naphthalene is more than three times higher than that of DPPH, the triplet quenching rate of benzophenone by naphthalene may be faster than the rate by DPPH. Thus, the triplet benzophenone is first quenched by naphthalene and then the triplet naphthalene is slowly quenched by DPPH to create CIDEP giving a net Em signal of DPPH. Consequently, it is expected that the CIDEP is created through the DPPH−triplet naphthalene encounter process at the high naphthalene concentration of 14 mM. A similar experiment was carried out for a benzophenone/phenanthrene mixture system with DPPH. In this experiment, a net Em signal was also observed when the T_1-T_1 energy transfer from benzophenone prepared triplet phenanthrene. The signal intensities were almost identical for benzophenone and benzophenone/phenanthrene systems. However, the decay rates of TR-ESR signal were different for the two systems, probably due to the different quenching rate constants by DPPH. The different time profiles enable us to distinguish the signals created by triplet benzophenone and by triplet phenanthrene, and suggest that CIDEP created by the DPPH−triplet phenanthrene system gives an Em phase TR-ESR signal. These experiments clearly indicate that the net Em signal observed in DPPH−naphthalene or −phenanthrene systems is created through the DPPH−triplet molecule encounter process.

Determination of k_q by Analysis of CIDEP in the DPPH−Triplet Coronene System. In this section, we determined the quenching rate constant of triplet coronene by DPPH in anisole by the Stern−Volmer analysis of the TR-ESR signal. Figure 7a shows the plots of relative signal intensities against the concentration of *trans*-stilbene. The intensity was normalized to the Abs signal intensity measured in the absence of *trans*-stilbene. The TR-ESR signal intensity, I(cor), due to the DPPH−coronene pair and I(stib) due to the DPPH−*trans*-stilbene pair are represented by the following equations:

$$I(\text{cor}) = I_0 \times (1 - \Phi) \tag{1}$$

$$I(\text{stib}) = I_\infty \times \Phi \tag{2}$$

where I_0 and I_∞ denote relative signal intensities at the *trans*-stilbene concentration zero and ∞, respectively. Φ is the quantum yield for triplet quenching by *trans*-stilbene given by the following equation:

$$\Phi = \frac{k_Q[\text{stilbene}]}{k_Q[\text{stilbene}] + k_q[\text{DPPH}]} \quad (3)$$

where k_Q and k_q are the quenching rate constants of triplet coronene by *trans*-stilbene and by DPPH, respectively. We neglected the unimolecular decay of triplet coronene since the lifetime of triplet coronene in the absence of dissolved oxygen is much longer than that of TR-ESR signals (<5 μs).

As seen in Figure 7a, the TR-ESR signal intensity approaches -0.55 with increasing *trans*-stilbene concentration and we determine the I_∞ value of -0.55. Therefore, the TR-ESR signal intensity, I, at a given concentration of *trans*-stilbene is described by the following equation:

$$I = I(\text{cor}) + I(\text{stib}) = 1 - 1.55 \times \Phi \quad (4)$$

From this equation with the I value, we determine the Φ values for each concentration of *trans*-stilbene. Equation 3 is rewritten as follows:

$$\frac{1}{\Phi} = 1 + \frac{k_q[\text{DPPH}]}{k_Q}\frac{1}{[\text{stilbene}]} \quad (5)$$

According to eq 5, we plot Φ^{-1} against $[\text{stilbene}]^{-1}$ as show in Figure 7b. From a least-squares fit of the plots, we obtain the slope of $(1.05 \pm 0.66) \times 10^{-3}$ M. The k_Q value of $(1.94 \pm 0.03) \times 10^9$ M^{-1} s^{-1} is determined by monitoring the transient absorption of triplet coronene in toluene. By considering the difference in diffusion rate constants of toluene and anisole,[14] we estimate the k_Q value of 8.64×10^8 M^{-1} s^{-1} in anisole. From the values of k_Q and the slope, and the concentration of DPPH (0.29 mM), the k_q value is estimated to be 3.1×10^9 M^{-1} s^{-1}. This value is slightly smaller than the diffusion rate constant in anisole (4.9×10^9 M^{-1} s^{-1}). Since the D_1 energy of DPPH (12200 cm^{-1}) is lower than the T_1 energy of coronene (19040 cm^{-1}),[14] the triplet−doublet energy transfer is exothermic and the k_q will be close to the diffusion-controlled rate constant.[16] The present result of the k_q value satisfies this feature.

The CIDEP Mechanism in the DPPH−Triplet Molecule System. The CIDEP observed in the present study are created upon the encounter of DPPH and the triplet molecule. Two independent mechanisms, RTPM[4,6] and ESPT,[9,13] are responsible for the CIDEP created in the RT systems. According to RTPM, which has been described before, CIDEP is created as far as triplet molecules exist in the system of interest. On the other hand, CIDEP creation due to ESPT requires the existence of spin-polarized triplet molecules. Usually, anisotropic S_1-T_1 intersystem crossing of organic compounds results in a non-Boltzman distribution with α-spin-enriched population.[17] The triplet molecule with non-Boltzman distribution encounters a free radical and the exchange of electron spin occurs between the triplet molecule and the free radical. During the exchange process, the α-spin enriched population of the triplet molecule is transferred to the free radical due to the conservation of spin angular momentum.[13] This process creates the Em phase CIDEP on the free radical. The spin-polarized triplet disappears rapidly due to spin−lattice relaxation processes. The spin−lattice relaxation time of the triplet is generally much shorter than the triplet lifetime. Hence, the creation of CIDEP by ESPT occurs in the early short period while that by RTPM takes place for a longer period.

Since most of the DPPH−triplet molecule systems studied in this work show net Em CIDEP, it is necessary to consider the occurrence of ESPT as a CIDEP creation mechanism. The spin relaxation time of triplet molecules in the liquid phase at room temperature is generally short due to the rapid tumbling motion. It is roughly estimated to be on the nanosecond order (the corresponding rate, $(1.0 \times 10^{8-9})$ s^{-1}).[3a,18,19] In the present experiments with low concentrations of DPPH, 0.3−0.7mM, the corresponding ESPT rate is estimated be $<7.7 \times 10^6$ s^{-1} assuming that ESPT occurs at a diffusion-controlled rate. Under our experimental conditions and applying estimated spin relaxation rates ($1.0 \times 10^{8-9}$ s^{-1}), at most 7.1% of triplet spin polarization could transfer to DPPH. Therefore, it is likely that the CIDEP created by ESPT is minor in the present DPPH−triplet molecule systems.

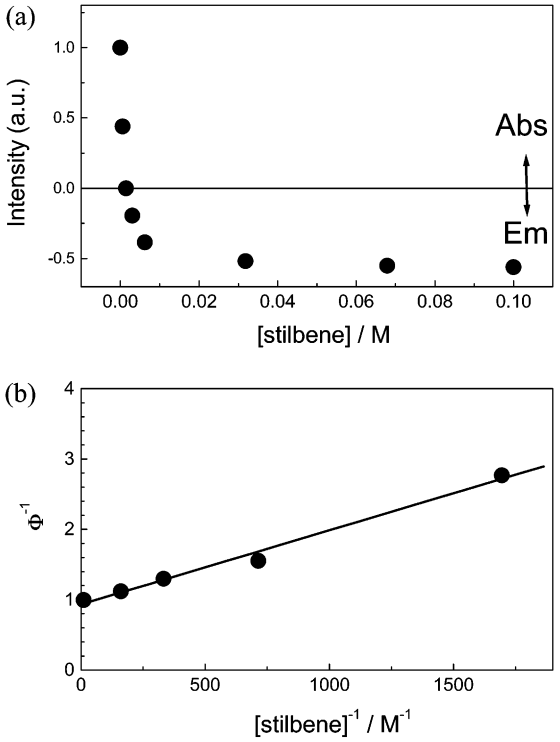

Figure 7. (a) A plot of TR-ESR signal intensities against *trans*-stilbene concentrations in the DPPH/coronene system. Signal intensities were obtained by integrating the time profiles of TR-ESR signals from 0 to 6 μs. The intensity is asymptotic to -0.55 (I_∞). (b) A Stern−Volmer plot of Φ^{-1} values against $[\text{stilbene}]^{-1}$. A least-squares fitting of the plot gives the slope value of $(1.05 \pm 0.66) \times 10^{-3}$ M.

To make sure that the Em CIDEP observed in the present work is not due to ESPT, we carried out the following two independent experiments; time profile measurements and simulation by Bloch and kinetic equations, and Stern−Volmer type quenching experiments. In RTPM and ESPT, the excited molecules that create CIDEP are triplet molecules with thermally- and non-Boltzman-distributions, respectively. The thermally populated triplet molecules decay on the microsecond order, while the spin-polarization of the triplet molecule relaxes on the nanosecond order. This difference results in the different time evolutions of TR-ESR signals. Therefore, the time profile of the TR-ESR signal may tell us which mechanism dominates in the process to create the observed CIDEPs. Similary, the quenching experiments on the TR-ESR signal intensities provide us information on the available CIDEP mechanism through a kinetic parameters of triplet lifetime determined by the Stern−Volmer analysis.

Time Profile Analysis. First, we simulate the time profiles of TR-ESR signals ($\propto M_y$: magnetization along the y-axis) by Bloch and kinetic equations considering RTPM as a CIDEP mechanism. Bloch equations modified with additional terms to allow for chemical kinetics are given by

$$\frac{dM_y}{dt} = -\frac{M_y}{T_2} + \omega_1 M_z \quad (6)$$

$$\frac{dM_z}{dt} = -\omega_1 M_y - \frac{(M_z - P_{eq}[\mathrm{DPPH}])}{T_1} + P_n k_{\mathrm{CIDEP}}[\mathrm{DPPH}][\mathrm{triplet}] \quad (7)$$

$$\frac{d[\mathrm{triplet}]}{dt} = \Phi_{\mathrm{ISC}} k_f[\mathrm{Singlet}^*] - (k_T + k_q[\mathrm{DPPH}])[\mathrm{triplet}] \quad (8)$$

where P_n and k_{CIDEP} are spin polarization factor and the rate constant for CIDEP creation, respectively. Φ_{ISC} and k_f are the quantum yield for S_1-T_1 intersystem crossing and fluorescence decay rate of the S_1 molecule. The k_T is the triplet decay rate in the absence of DPPH. All the other symbols follow their standard notation. The T_2 value is estimated to be 200 ns or less from the line width of the CW-ESR spectra determined by simulation of hyperfine structure. In the simulation, we used the T_2 value of 200 ns. The ω_1 value is $(1-3) \times 10^6$ rad s^{-1}, depending on the microwave power in our ESR cavity. The initial concentration of the excited molecule was 0.01 mM, estimated from laser power. Since DPPH signals due to thermal distribution were not observed, we take the appropriate $P_n \times k_{\mathrm{CIDEP}}$ value which is large enough to neglect the term of P_{eq} in eq 7. The k_T value is 1×10^5 s^{-1} or less in solution with Ar bubbling. The k_T value of 1×10^5 s^{-1} is small enough to perform simulation with eq 8 since the triplet quenching rates by DPPH are expected to be much faster than 1×10^5 s^{-1}. Taking an example of coronene, we have already determined the $k_q = 3.1 \times 10^9$ M^{-1} s^{-1} and the k_q[DPPH] value becomes 1.6×10^6 s^{-1}. We simulate the time profiles by eqs 6−8 and estimated the T_1 value of DPPH and k_q values for each system. Figure 8a shows the time profiles of TR-ESR signals measured in the DPPH−triplet coronene system, together with the simulated curves (solid) using three different k_q values. As seen in Figure 8a, the best simulation is obtained with the k_q value of 2.5×10^9 M^{-1} s^{-1}. The T_1 value is estimated to be about 300 ns. The k_q value estimated by this simulation is close to 3.1×10^9 M^{-1} s^{-1} determined by the Stern−Volmer analysis of CIDEP intensities vs DPPH concentration. This result suggests that the DPPH−triplet molecule encounter process creates the CIDEP. Figure 8b shows the time profile of a TR-ESR signal measured in the DPPH−triplet benzophenone system together with the simulated curves (solid) using three different k_q values. The best fitting is obtained by the k_q value of 1.6×10^9 M^{-1} s^{-1}. Similar simulations were carried out for other CIDEP time profiles of the DPPH−triplet molecule systems, and the resultant k_q values are listed in Table 2. It is noteworthy that the k_q values are mostly on the order of 10^9 M^{-1} s^{-1}, that is close to the diffusion rate constants in these solvents. The lowest triplet energy of molecules used here is 11700 cm^{-1} of TPP and all the others are much higher.[14] Since the D_1 energy of DPPH is low (12200 cm^{-1}), the triplet quenching processes by DPPH studied here are mostly exothermic. This is why the k_q values are close to the diffusion rate constants. The time profiles are well simulated with the k_T value of 1.0×10^5 s^{-1}. This result suggests that the triplet molecules are not spin-polarized but in thermal population. The CIDEP mechanism is concluded to be RTPM.

Additionally, we simulate time profiles on the basis of ESPT to confirm that ESPT does not reproduce time profiles. In this model calculation, the triplet molecule must be spin-polarized and thus the concentration of the triplet in eqs 7 and 8 is replaced by the concentration of the spin-polarized triplet. In eq 8, k_T is replaced by the sum of triplet spin−lattice relaxation rate, $1/T_1^t$ and the k_T values. However, we neglected the latter because the k_T of the triplet without dissolved oxygen is much smaller than $1/T_1^t$. Hence, the kinetic eq 8 is rewritten as

$$\frac{d[\mathrm{triplet}^*]}{dt} = -(1/T_1^t + k_q[\mathrm{DPPH}])[\mathrm{triplet}^*] \quad (9)$$

where triplet* denotes a spin-polarized triplet molecule. In the simulation, we adopted *a* T_1 value of 300 ns, T_1^t value of 10 ns, and k_q values of 3.1×10^9 M^{-1} s^{-1} for coronene and 1.6×10^9 M^{-1} s^{-1} for benzophenone. The simulated time profiles by

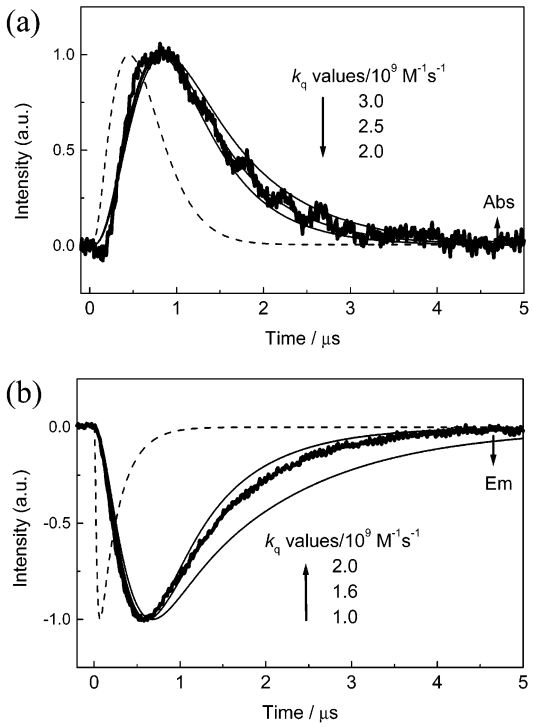

Figure 8. Time profiles of the TR-ESR signal of DPPH observed with the 355 nm laser excitation of (a) DPPH−triplet coronene system in anisole and (b) DPPH−triplet benzophenone system in benzene. The concentrations of samples were (a) DPPH(0.508 mM) and coronene-(3.65 mM) and (b) DPPH(0.58 mM) and benzophenone(74 mM). Solid simulation curves were calculated according to the Bloch and kinetic eqs 6−8 with various k_q values. Dotted simulation curves were calculated according to the Bloch and kinetic eqs 6, 7, and 9 with k_q values of 3.1×10^9 M^{-1} s^{-1} (coronene) and 1.6×10^9 M^{-1} s^{-1} (benzophenone). See the text for details. The S_1 lifetime of 240 ns was considered in the simulation of the DPPH−coronene system. The ω_1 value of 3×10^6 rad s^{-1} was used in both simulations.

TABLE 2: The k_q Values Estimated by the Simulation of Time Profiles of TR-ESR Signals with Bloch and Kinetic Equations

triplet molecules (solvent)	$k_q/10^9$ M^{-1} s^{-1}
2-acetonaphthone (benzene)	1.1
benzil (benzene)	0.8
benzophenone (benzene)	1.6
4-chlorobenzophenone (benzene)	2.6
coronene (anisole)	2.5
fluoranthene (toluene)	4.0
9-fluorenone (benzene)	2.3
naphthalene (benzene)	0.7
1-nitronaphthalene (toluene)	2.5
phenanthrene (benzene)	1.4
phenazine (benzene)	0.6
tetraphenylporphine (toluene)	2.5

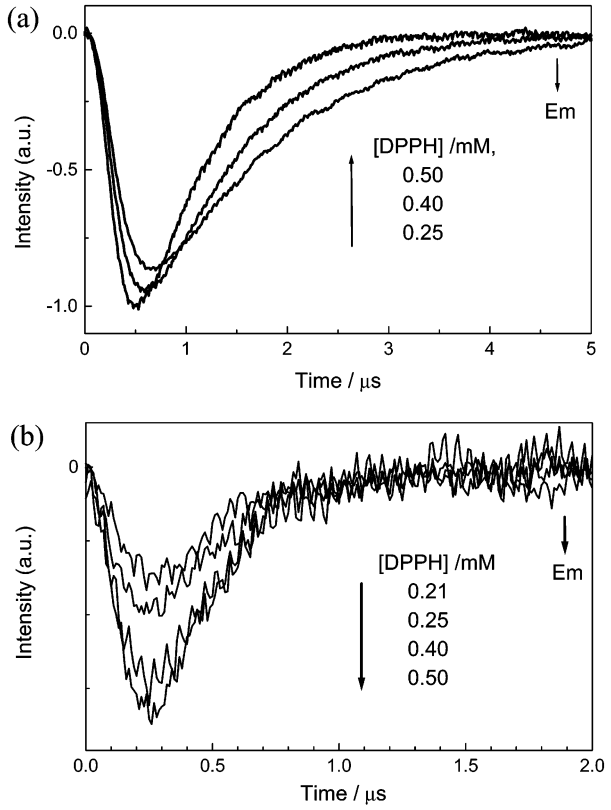

Figure 9. (a) Time profiles of the TR-ESR signal of DPPH observed with 355 nm excitation of the DPPH/9-fluorenone system in benzene with various concentrations of DPPH. The sample solutions were (a) bubbled by Ar to remove dissolved O_2 and (b) air-saturated.

this model are shown in Figure 8 by dotted lines. The simulation curves apparently fail to reproduce the observed time profiles. For the best fitting, the T_1^t value must be more than 5 μs, that is unlikely for the triplet molecule in the solution at 293 K. This simulation suggests that the observed CIDEP is not created by ESPT. Similar results were obtained for all the decay profiles studied here, and thus we consider that the CIDEP studied is not due to ESPT but is due to RTPM.

Stern−Volmer Analysis. Stern−Volmer type quenching experiments were carried out to check if the measured CIDEP intensity could be reasonably explained by RTPM as the CIDEP mechanism. In this analysis, we measured the CIDEP intensity, I, obtained by integration of the time profile of TR-ESR signal. The CIDEP intensities are analyzed by using the following Stern−Volmer type equation:

$$\frac{1}{\phi_{\mathrm{CIDEP}}} = 1 + \frac{k_t}{k_q}\frac{1}{[\mathrm{DPPH}]} \qquad (10)$$

The ϕ_{CIDEP} is calculated by $1/\phi_{\mathrm{CIDEP}} = I(\infty)/I$, where $I(\infty)$ denotes the CIDEP intensity extrapolated to infinite DPPH concentration. It is expected that DPPH quench all triplet molecules at that limiting condition. The k_t corresponds to k_T for RTPM and $1/T_1^t$ for ESPT.

Figure 9a and 9b shows TR-ESR time profiles of DPPH in DPPH−triplet 9-fluorenone system with various DPPH concentrations without and with dissolved O_2, respectively. The dissolved O_2 shortens the lifetime of triplet molecules, and thus the remarkable difference between the two figures is the lifetime of the triplet decay rate in the absence of DPPH. In Figure 9a, decay time is prolonged with decreasing DPPH concentration. In Figure 9b, signal intensity changes drastically with DPPH

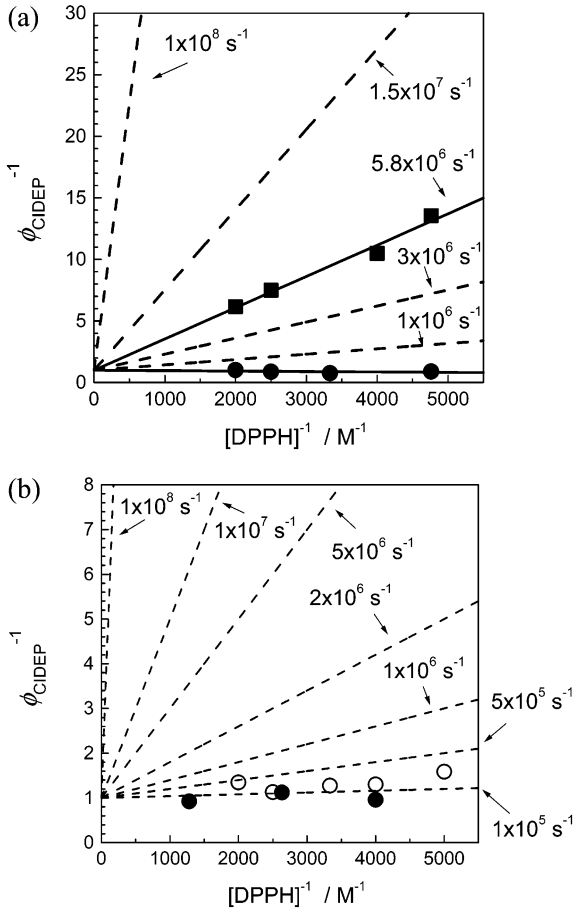

Figure 10. Stern−Volmer plots of $\phi_{\mathrm{CIDEP}}^{-1}$ against $[\mathrm{DPPH}]^{-1}$ for DPPH−triplet systems, together with simulation lines with various k_t values depicted in each line. (a) The CIDEP intensities were measured for the DPPH−triplet 9-fluorenone system under air-saturated conditions (rectungular) and under air-removed conditions by Ar bubbling (circle). (b) The CIDEP intensities were measured for the DPPH−triplet TPP (open circle) and DPPH−triplet coronene (closed circle) systems under air-removed conditions.

concentration while the time profile is almost identical. We measured time profiles against various concentrations of DPPH for these two distinct conditions. Figure 10a shows the plots of $\phi_{\mathrm{CIDEP}}^{-1}$ against $[\mathrm{DPPH}]^{-1}$ obtained from the time profiles (Figure 9). To obtain $\phi_{\mathrm{CIDEP}}^{-1}$ values, we first plotted I^{-1} values vs $[\mathrm{DPPH}]^{-1}$ and determined $I(\infty)$ from the intercept of the plot. Then, we calculated $\phi_{\mathrm{CIDEP}}^{-1}$ values for each concentration of DPPH. As shown in the Figure 10a, both plots with and without dissolved oxygen are on the straight lines, which means than eq 10 stands for these sets of data.

First we examine the results in the presence of dissolved O_2. From the slope value of the plot and the k_q value of 2.3×10^9 M^{-1} s^{-1}, we obtained a k_t value of 5.8×10^6 s^{-1}. The quenching rate constant of triplet benzophenone by O_2 in benzene[20] is 2.3×10^9 M^{-1} s^{-1}, and we assumed this value for that of 9-fluorenone. The concentration of dissolved O_2 is 1.9 mM at 293 K, according to the literature,[14] and the triplet decay rate k_T is calculated to be 4.4×10^6 s^{-1}. Judging that the estimated k_T value includes much assumption, we consider that the k_t value determined by eq 10 of the plot is similar to the estimated k_T value.

Next, we analyze the result without dissolved O_2. The slope value in Figure 10a is very small and we refrain from determining the k_t value. We draw several simulated lines with k_t values from 1.0×10^8 s^{-1} to 1.0×10^6 s^{-1} and k_q of $2.3 \times$

TABLE 3: Sign of *J*- and Estimated $\Delta G(r)$ Values in DPPH−Triplet Systems

molecules	sign of *J*-value	$\Delta E(T_1)$ kcal mol^{-1}	$E_{1/2}^{red}$ [V] vs SCE	$\Delta G(r)$ value kcal mol^{-1}
9,10-diphenylanthracene	−	41.8	−1.94	13.3
anthracene	−	42.7	−1.95	12.6
pyrene	−	48.2	−2.09	10.4
2-methylnaphthalene	−	60.7	−2.58	9.17
E-stilbene	−	50.0	−2.08	8.35
naphthalene	−	60.9	−2.49	6.90
chrysene	−	56.6	−2.25	5.67
phenanthrene	−	61.9	−2.44	4.75
coronene	+	54.4	−2.07	3.71
tetraphenylporphine	−	32.9	−1.08	2.35
acridine	−	45.4	−1.62[a]	2.33
quinoxaline	−	60.7	−2.11[a]	−1.67
fluoranthene	−	52.9	−1.74	−2.40
diphenylacetylene	−	62.6	−2.11	−3.58
phenazine*	−	44.4	−1.23[a]	−5.65
2-acetonaphthone	−	59.5	−1.72[b]	−9.47
9-fluorenone	−	50.4	−1.29	−10.2
4,4-dimethoxybenzophenone	−	70.0	−2.02[a]	−13.1
4,4-dimethylbenzophenone	−	68.8	−1.90[a]	−14.6
benzophenone	−	68.6	−1.83[a]	−16.0
4-chlorobenzophenone	−	68.3	−1.75[a]	−17.6
1-nitronaphthalene	−	54.9	−0.97	−22.2
2-nitronaphthalene	−	56.9	−0.98	−23.9
benzil	−	53.4	−0.71[b]	−26.6

[a] The $\Delta E(T_1)$ and $E_{1/2}^{red}$ values are from ref 14. [b] Solvent for $E_{1/2}^{red}$ values is *N*,*N*-dimethylformamide, except (a) acetonitrile and (b) ethanol/water(1:1 vol) mixture.

10^9 M^{-1} s^{-1}. Theoretically calculated spin relaxation rate $1/T_1^t$ is more than 1.0×10^8 s^{-1}, and we obviously fail to reproduce data points by introducing this value as k_t value in eq 10. Though the data points scatter, the simulation suggests the k_t value without dissolved O_2 is much smaller than 1×10^6 M^{-1} s^{-1}. This value is reasonable for 9-fluorenone triplet decay rate k_T in benzene without O_2, but it is too small for $1/T_1^t$.

According to these sets of the results, we conclude that the triplet 9-fluorenone that creates CIDEP on DPPH by the encounter process is not a spin-polarized but rather a thermally populated triplet molecule. Similar experiments were performed on DPPH−triplet coronene and DPPH−triplet TPP systems and the plots for ϕ_{CIDEP}^{-1} without O_2 are shown in Figure 10b. As is clearly seen in the plots, estimated k_t values for triplet coronene and TPP are smaller than 5×10^5 M^{-1} s^{-1}. This also suggests that the CIDEP is dominantly created by a thermally populated triplet. These Stern−Volmer type experiments also indicate that ESPT is a minor process in the CIDEP creation and support that the CIDEP is created by RTPM.

Sign of the *J*-Value in DPPH−Triplet Molecule Systems. According to the analysis described above, it is found that CIDEP in various DPPH-excited molecule systems are created by RTPM of DPPH-triplet molecule encounter pairs. Therefore, we determined the sign of *J*-value from the phase of CIDEP and sign rule of RTPM as summarized in Table 3. All the DPPH−triplet molecule systems show a negative *J*-value except coronene that shows a positive *J*-value. This feature is mostly in accord with *J*-values in TEMPO−triplet molecule systems in which all the systems indicate a negative sign of *J*-value.

Previously, we reported that the *J*-value in RTP includes both contributions from exchange and intermolecular CT interactions.[8] We explain this briefly by a schematic diagram shown in Figure 11. ^{4}RTP^0 and ^{2}RTP^0 states are separated by exchange interaction and the *J*-value is negative at potential minimum, r_{RT} of RTP along the solvent coordinate as shown in Figure 11a. This was supported by the results of RTP in which the energy gap of RTP and intermolecular CT states is too large to

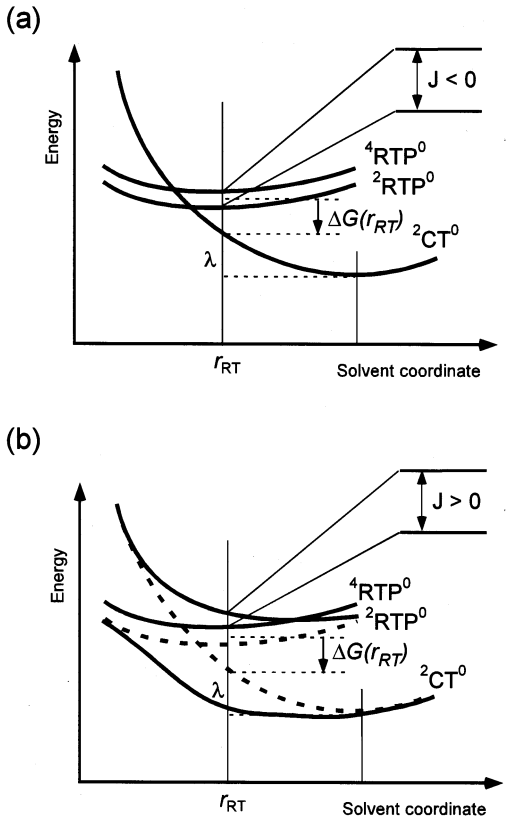

Figure 11. Schematic description of the energies of RTP and CT pair states along the solvent coordinate. RTP^0 states are split into the ^{2}RTP^0 and ^{4}RTP^0 states by exchange interaction. Zeemann splittings are excluded for both RTP^0 and CT^0 states. Electron correlation between ^{2}RTP^0 and ^{2}CT^0 states are (a) negligible giving $J < 0$ and (b) dominant giving $J > 0$.

bring about the perturbation on the RTP states. On the other hand, some RT systems with their intermolecular CT states closely locating near the RTP state indicate a positive sign of the *J*-value in the studies of galvinoxyl−triplet molecule systems. This is schematically shown in Figure 11b. The configuration interaction between RTP^0 and ^{2}CT^0 states causes energy shift of these states. We exclude the ^{4}CT^0 state in the discussion because the ^{4}CT^0 state energy is much higher than that of the ^{2}CT^0 state as discussed previously.[8] If the ^{2}CT^0 state locates below the RTP^0 state, the ^{2}RTP state is blue-shifted against the ^{2}RTP^0 state, while no energy shift is expected for the ^{4}RTP^0 state because of smaller configuration interaction between the states of different spin multiplicity. If the effect causing blue-shift of the ^{2}RTP^0 state overcomes the effect of exchange interaction, the sign of the *J*-value could be positive[8] as shown in Figure 11b.

To examine the effect of the CT state on the *J*-value, we first estimate the energy gap, ΔG, between the RTP^0 and CT^0 states by the following equation:

$$\Delta G(r) = G(\mathrm{CT}^0) - G(\mathrm{RTP}^0) = \{E_{1/2}{}^{ox}(\mathrm{DPPH}) - E_{1/2}{}^{red}(\mathrm{triplet}) + \Delta E_{corr}\} + \{\lambda(r) - E_{coulomb}(r)\} - \Delta E(T_1) \quad (11)$$

$E_{1/2}{}^{ox}$(DPPH) and $E_{1/2}{}^{red}$(triplet) mean half-wave redox potentials of DPPH and molecules used as triplet. ΔE_{corr} represents the correction values of redox potentials for different solvents. $\lambda(r)$ and $E_{coulomb}(r)$ are solvent reorganization and Coulomb energies of CT pairs, respectively, at a given radical−triplet

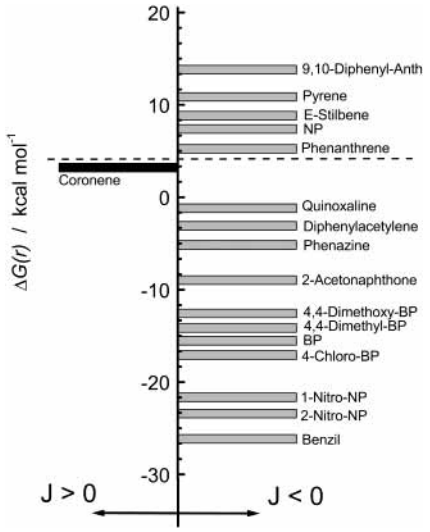

Figure 12. A Plot of the sign of the *J*-value against ΔG for various DPPH−triplet molecule pairs. The values are listed in Table 3. Abbreviations are Anth, anthracene; NP, naphthalene; and BP, benzophenone.

distance, *r*. The half-wave potential for oxidation of DPPH was reported to be +0.693 V vs SCE in acetonitrile.[21] Since redox potentials reported are obtained in very polar solvents ($\epsilon > 30$), we added ΔE_{corr} of 14.86 kcal mol^{-1} calculated by the Born equation for solvation energies of the anion and cation. Parameters used for this correction are an ion radius of 3.5 Å, dielectric constants ϵ of 35.94 and 2.284 for acetonitrile and benzene, respectively. Our value (14.86 kcal mol^{-1}) is close to the ΔE_{corr} value of 16.1 kcal mol^{-1} reported for the correction between acetonitrile and cyclohexane solutions.[22] The $\lambda(r)$ for benzene of ca. 0.28 kcal mol^{-1} is calculated by the formula derived by R. A.Marcus[23] assuming $r_A = r_D = 3.5$ Å, and $r_{AD} = 7$ Å. The $E_{coulomb}(r)$ was calculated to be ca. 20.75 kcal mol^{-1} assuming $r_{AD} = 7$ Å. The estimated $\Delta G(r)$ values are summarized in Table 3, together with $\Delta E(T_1)$[14] and reduction potentials[14,24] for a series of RT systems. Figure 12 shows relation between the $\Delta G(r)$ and the sign of *J*-values in DPPH−triplet molecule systems. The plots covers the $\Delta G(r)$ range from − 25 to 15 kcal mol^{-1} and the sign of the *J*-value is represented by black (+) and gray (−) bars. It might be mentioned here that a DPPH−triplet coronone system presents a uniquely positive *J*-value and belongs to a system with the $\Delta G(r)$ value being close to zero.

For the purpose of understanding the relation between the $\Delta G(r)$ values and the sign of the *J*-value, similar plots for three different radicals (galvinoxyl, DPPH, and TEMPO) were described in Figure 13. In the galvinoxyl−triplet molecule systems, positive *J*-values are found in the systems with $\Delta G(r)$ values from −14 to −4 kcal mol^{-1}. This feature has already been explained by the effect of the intermolecular CT state. The remarkable difference between the DPPH−triplet molecule and galvinoxyl−triplet molecule systems is that the positive *J*-values are found only in a coronene system in DPPH while several systems with molecules such as naphthalene, biphenyl, quinoxaline, and coronene have positive *J*-values in galvinoxyl.[8] The $\Delta G(r)$ value of the DPPH−coronene system is calculated to be +3.7 kcal mol^{-1}, which means that the $^2CT^0$ state is slightly higher in energy than the RTP^0 states. If the negative−positive sign change of *J*-value is caused by the effect of a near-lying CT state, the $\Delta G(r)$ value is expected to be negative. Since our $\Delta G(r)$ estimation includes a large uncertainty, we consider that the value of 3.7 kcal mol^{-1} is within the estimation error and that the real $\Delta G(r)$ value for the DPPH−coronene system is not positive. Another interesting fact is that no RT system with a positive sign of the *J*-value was found in TEMPO−triplet molecule systems with a range of $\Delta G(r)$ values from −35 to 25 kcal mol^{-1}. Even though the system has a small and negative $\Delta G(r)$ value, the *J*-value does not become positive. This result suggests that the contribution of exchange interaction to the sign of the *J*-value is more significant than that of CT interaction in TEMPO−triplet molecule systems. Similary, exchange interaction dominantly contributes to the sign of the *J*-value in DPPH−triplet molecule systems since most of the systems show negative *J*-value.

It is interesting to discuss the reason the CT interaction is more dominant than exchange interaction in the DPPH−triplet

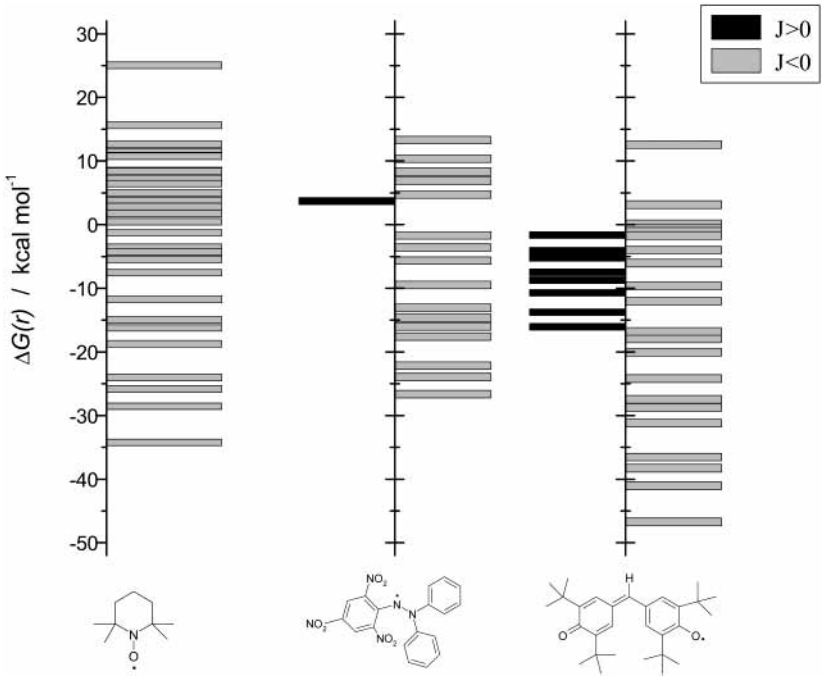

Figure 13. Plots of the sign of the *J*-value against ΔG for galvinoxyl−, DPPH−, and TEMPO−triplet molecule pairs.

coronene system. DPPH and coronene have large π orbitals and the structures are close to planar. In this particular system, both encounter complexes with CT and RTP states might show a sandwich structure and the matrix element and Franck−Condon overlap between these states may be large. This could be one of the reasons that the CT interaction in the DPPH−triplet coronene system becomes dominant giving a positive *J*-value.

On the contrary to the radical−ion pairs in which the sign of the *J*-value is totally controlled by the CT effect,[26] the balance between the exchange and CT effects is definitely important in the sign of the *J*-value of RTP. Extended studies on the *J*-value utilizing various kinds of free radicals are now in progress to understand the effect of CT interaction in RTP and electron correlation between RTP^0 and CT^0 states.

Acknowledgment. We express our thanks to Prof. Kinichi Obi for his encouragement in this study. The present work is partly defrayed by the Grant-in-Aid for Scientific Research (Nos. 13740327 and 13127202) from the Ministry of Education, Sports, Science and Culture of Japan. A part of this study was performed using one of on-campus cooperative research facilities in Tokyo Institute of Technology, 'a pulsed ESR system'.

References and Notes

(1) (a) Buckley, C. D.; Hunter, D. A.; Hore, P. J.; McLauchlan, K. A. *Chem. Phys. Lett.* **1987**, *133*, 307. (b) Tominaga, K.; Yamauchi, S.; Hirota, N. *J. Chem. Phys.* **1990**, *92*, 5175.

(2) (a) Murai, H.; Sakaguchi, Y.; Hayashi, H.; I'Haya, Y. J. *J. Phys. Chem.* **1986**, *90*, 113. (b) Closs, G. L.; Forbes, M. D. E.; Norris, J. R. *J. Phys. Chem.* **1987**, *91*, 3592.

(3) For examples, (a) Willigen, H. van; Levstein, P. R.; Ebersole, M. H. *Chem. Rev.* **1993**, *93*, 173. (b) Terazima, M.; Maeda, K.; Azumi, T.; Tanimoto, Y.; Okada, N.; Itoh, M. *Chem. Phys. Lett.* **1989**, *164*, 562. (c) Nakagawa, K.; Katsuki, A.; Tero-Kubota, S.; Tsuchihashi, N.; Fujita, T. *J. Am. Chem. Soc.* **1996**, *118*, 5782. (d) Kawai, A.; Shikama, A.; Mitsui, M.; Obi, K. *Bull. Chem. Soc. Jpn.* **2001**, *74*, 1203.

(4) (a) Blättler, C.; Jent, F.; Paul, H. *Chem. Phys. Lett.* **1990**, *166*, 375. (b) Goudsmit, G−H.; Paul, H.; Shushin, A. I. *J. Phys. Chem.* **1993**, *97*, 13243.

(5) (a) Kawai, A.; Okutsu, T.; Obi, K. *J. Phys. Chem.* **1991**, *95*, 9130. (b) Kawai, A.; Obi, K. *J. Phys. Chem.* **1992**, *96*, 5701. (c) Kobori, Y.; Mitsui, M.; Kawai, A.; Obi, K. *Chem. Phys. Lett.* **1996**, *252*, 355. (d) Kawai, A.; Obi, K. *J. Phys. Chem.* **1992**, *96*, 52. (e) Kobori, Y.; Kawai, A.; Obi, K. *J. Phys. Chem.* **1994**, *98*, 6425. (f) Mitsui, M.; Takada, K.; Kobori, Y.; Kawai, A.; Obi, K. *Chem. Phys. Lett.* **1996**, *262*, 125. (g) Kawai, A.; Mitsui, M.; Kobori, Y.; Obi, K. *Appl. Magn. Reson.* **1997**, *12*, 405.

(6) Kawai, A.; Obi, K. *Res. Chem. Intermed.* **1993**, *19*, 866.

(7) (a) I'Haya, Y. J.; Kanosue, S. *Chem. Phys. Lett.* **1993**, *216*, 231. (b) Turro, N. J.; Khudyakov, I. V.; Dwyer, D. W. *J. Phys. Chem.* **1993**, *79*, 10530. (c) Fujisawa, J.; Ishii, K.; Ohba, Y.; Iwaizumi, Y.; Yamauchi, S. *J. Phys. Chem.* **1995**, *99*, 17082. (d) He, G.; Chen, C.; Yang, J.; Xu, G. *J. Phys. Chem. A* **1998**, *102*, 2865.

(8) (a) Kawai, A.; Shibuya, K.; Obi, K. *Appl. Magn. Reson.* **2000**, *18*, 343. (b) Kawai, A.; Watanabe, Y.; Shibuya, K. *Mol. Phys.* **2002**, *100*, 1225.

(9) Blank, A.; Levanon, H. *J. Phys. Chem. A* **2000**, *104*, 794.

(10) (a) Ohara, K.; Hirota, N. *Bull. Chem. Soc. Jpn.* **1996**, *69*, 1517. (b) Kawai, A.; Yamamoto, T.; Okutsu, T.; Obi, K. *Bull. Chem. Soc. Jpn.* **1999**, *72*, 2625. (c) Okutsu, T.; Ooyama, M.; Tani, K.; Hiratsuka, H.; Kawai, A.; Obi, K. *J. Phys. Chem. A* **2001**, *105*, 3741.

(11) (a) Carrington, A.; McLachlan, A. D. *Introduction to Magnetic Resonance with Application to Chemistry and Chemical Physics*; Harper and Row: New York, 1967. (b) Devan, L.; Bowman, M. K. *Modern Pulsed and Continuous-Wave Electron Spin Resonance*; John Wiley and Sons: New York, 1990. (c) Muss, L. T.; Atkins, P. W.; McLauchlan, K. A.; Pedersen, J. B. *Chemically Induced Magnetic Polarization*; D. Reidel Publishing Company: Dordrecht-Holland and Boston-USA, 1977. (d) Molin, Y. N. *Spin Polarization and Magnetic Effects in Radical Reactions*; Wiley-Interscience: New York, 1973.

(12) (a) Shushin, A. I. *Z. Phys. Chem.* **1993**, *182*, 9. (b) Shushin, A. I. *Chem. Phys. Lett.* **1993**, *208*, 173. (c) Shushin, A. I. *Chem. Phys. Lett.* **1999**, *313*, 246.

(13) (a) Imamura, T.; Onitsuka, O.; Obi, K. *J. Phys. Chem.* **1986**, *90*, 6741. (b) Fujisawa, J.; Ohba, Y.; Yamauchi, S. *J. Phys. Chem A* **1997**, *101*, 434.

(14) Murov, S. L.; Carmichael, I.; Hug, G. L. *Handbook of Photochemistry*; Marcel Dekker: New York, 1993.

(15) *J. Phys. Chem. Ref. Data* **1986**, *15*.

(16) Porter, G.; Topp, M. R. *Proc. R. Soc. London, Ser. A* **1970**, *315*, 163.

(17) *Appl. Spectrosc. Rev.* **1981**, *17*.

(18) Atkins, P. W.; Evans, G. T. *Mol. Phys.* **1974**, *27*, 1633.

(19) Turro, N. J.; Koptyung, I. V.; Willigen, H. V.; McLauchlan, K. A. *J. Magn. Reson., Ser. A* **1994**, *109*, 121.

(20) *Handbook of Organic Photochemistry*; Scaiano, J. C., Ed.; CRC Press, Inc.: Boca Raton, FL, 1989.

(21) Solon, E.; Bard, A. J. *J. Am. Chem. Soc.* **1964**, *86*, 1926.

(22) Chen, J. M.; Ho, T−I.; Mon, C−Y. *J. Phys. Chem.* **1990**, *94*, 2889.

(23) (a) Marcus, R. A. *Int. J. Chem. Kinet.* **1981**, *13*, 865. (b) Marcus, R. A. *J. Chem. Phys.* **1956**, *24*, 966. (c) Marcus, R. A. *J. Chem. Phys.* **1957**, *26*, 867.

(24) Mann, C. K.; Barnes, K. K. *Electrochemical reactions in nonaqueous systems*; Marcel Dekker, Inc.: New York, 1970.

(25) Valgimigli, L.; Ingold, K. U.; Lusztyk, J. *J.Org.Chem.* **1996**, *61*, 7947.

(26) (a) Sekiguchi, S.; Kobori, Y.; Akiyama, K.; Tero-Kubota, S. *J. Am. Chem. Soc.* **1998**, *120*, 1325. (b) Kobori, Y.; Sekiguchi, S.; Akiyama, K.; Tero-Kubota, S. *J. Phys. Chem. A* **1999**, *103*, 5416.